MNRAS **000**, 000–000 (0000) Preprint 2 June 2017 Compiled using MNRAS LATEX style file v3.0

Tilting Styx and Nix but not Uranus with a Spin-Precession-Mean-motion resonance

Alice C. Quillen[1], & Yuan-Yuan Chen[1], and?

order and author list to be determined
[1]*Department of Physics and Astronomy, University of Rochester, Rochester, NY 14627 USA*

2 June 2017

ABSTRACT
A Hamiltonian model is constructed for the spin axis of a planet perturbed by a nearby planet and both are in orbit about star. We expand the perturbation to first order in inclination and eccentricity, finding terms describing spin resonances involving the spin precession rate and the two planetary mean motions. Convergent planetary migration allows the spinning planet to be captured into spin resonance. With the spinning body near zero initial obliquity, the spin resonance can lift its obliquity to near 90 degrees if the resonance to first order in inclination dominates, whereas it could be lifted near 180 degrees if zeroth order or first order terms in eccentricity dominate. Past capture into such a spin resonance could give an alternative non-collisional scenario accounting for Uranus's high obliquity. However we find that the planet migration rate must be so slow that this mechanism cannot be responsible for Uranus's high obliquity. Our Hamiltonian model explains how Styx and Nix can be tilted to high obliquity via outward migration of Charon, a phenomenon previously seen in numerical simulations.

Keywords: Planets and satellites: dynamical evolution and stability, celestial mechanics, Planets and satellites: individual: Styx, Planets and satellites: individual: Nix

To do: Drift within MMR. Why is the spin resonance drifting with evolution in MMR?

1 INTRODUCTION

Resonances involving planet or satellite spin can cause chaotic tumbling, prevent a body from tidally despinning or affect obliquity. Mercury was captured into a spin-orbit resonance, with spin a half integer multiple of its mean motion, (e.g., Goldreich & Peale 1966; Noyelles et al. 2014) whereas Hyperion is chaotically tumbling due to spin-orbit resonance overlap (Wisdom et al. 1984). Secular spin-orbit resonances occur when the period of precession of the spin axis of a planet is commensurate with one of the periods in the secular variation of the orbit (Ward 1974). These cause chaotic obliquity variations in Mars (Ward 1973, 1974; Laskar & Robutel 1993; Touma & Wisdom 1993). Capture into the secular spin resonance connected to the vertical secular eigenfrequency associated with Neptune may have tilted Saturn's obliquity to its current value of 26.7° (Ward & Hamilton 2004; Hamilton & Ward 2004). For an object in orbit about a binary, spin-binary resonance involves a commensurability between the binary mean motion, the orbital mean motion and the body's spin (Correia et al. 2015).

Our numerical study of obliquity evolution of Pluto and Charon's minor satellites, showed another type of spin resonance (Quillen et al. 2017). We found that a commensurability involving a mean motion resonance between Charon and a minor satellite and the satellite's spin precession rate could influence its obliquity (Quillen et al. 2017). For satellite Styx, near a 3:1 mean motion resonance with Charon, we saw obliquity variations when the angles

$$\phi_{s1} = 3\lambda_{Styx} - \lambda_{Charon} - \phi_{Styx} - \Omega_{Styx}$$
$$\phi_{s2} = 3\lambda_{Styx} - \lambda_{Charon} - 2\phi_{Styx} \quad (1)$$

where librating about constant values rather than circulating. Here λ_{Styx} and λ_{Charon} are the mean longitudes of Styx and Charon and Ω_{Styx} is the longitude of the ascending node of Styx, and orbital elements are measured with respect to Pluto or the center of mass of the Pluto/Charon binary, not the Sun. The precession angle ϕ_{Styx} describes the orientation of Styx's spin axis. The New Horizons Mission found that Pluto and Charon's minor satellites, Styx, Nix, Kerberos and Hydra have not tidally spun down to near synchronous rotation (Weaver et al. 2016). Quillen et al. (2017) proposed that a spin resonance involving a mean motion resonance between Charon and a minor satellite and the satellite's spin precession rate, when drifting due to an outwards migrating Charon, might account for the high, near 90° obliquities discovered by the New Horizons Mission (Weaver et al. 2016) of all four of Pluto and Charon's minor satellites, Styx, Nix, Kerberos and Hydra. Quillen et al. (2017) suggested that the minor satellite current obliquities need not be primordial.

Table 1. List of Symbols

a	semi-major axis
e	orbital eccentricity
I	orbital inclination
Ω	longitude of the ascending node
ω	argument of pericenter
M	mean anomaly
$\varpi = \omega + \Omega$	longitude of pericenter
$\lambda = M + \varpi$	mean longitude
M_*	mass of central star
n	mean motion
$\hat{\mathbf{n}}$	orbit normal unit vector
$\hat{\mathbf{s}}$	spin direction unit vector
C, A	moments of inertia of oblate planet
w	spin angular rotation rate of planet
α_s	spin precession rate
α	ratio of semi-major axes
$\mathbf{T}$	torque vector
r	orbital radius
ϕ	spin precession angle
θ	obliquity angle
$s \approx I/2$	used in low inclination expansions
R	spinning planet's equatorial radius
J_2	second zonal gravity harmonic for the spinning planet
q_s	normalized quadrupole coefficient of satellite system
l_s	normalized angular momentum of satellite system
λ_C	normalized moment of inertia about principal axis
p	canonical momentum variable, a function of obliquity
Δ	distance between perturber and spinning body
ψ, Ψ	angles used in expansion of disturbing function
$b_s^{(j)}(\alpha)$	Laplace coefficient
j	resonance index
ϵ	resonance strength in a Hamiltonian model
ν	distance to resonance in a Hamiltonian model
$c_0^j, c_s^j, c_{s'}^j$	coefficients used to compute spin resonance strengths
$c_{e1}^j, c_{e'1}^j$	"
$c_{e3}^j, c_{e'3}^j$	"
β	"

As we were lacking a model for this type of spin resonance strength, we were unable to assess its strength or even identify which type of resonant angle was likely to be most important for each of Pluto and Charon's minor satellites. We address this issue here with the development of a Hamiltonian model for this spin resonance in section 2. In section 3 we explore resonance capture by allowing the resonance in our Hamiltonian model to drift. In section 4 we apply our model to Pluto and Charon's minor satellites.

Uranus also has a high obliquity, of 98°. Could a similar spin resonance have tilted Uranus during a previous time when Uranus was in or near a mean motion resonance with another giant planet? Using the Hamiltonian model of sections 2 and 3 we answer this question in section 5. To aid the reader a list of symbols is included in Table 1.

2 SPIN EVOLUTION

A spinning oblate planet in orbit about a central mass M_* that has spin axis, $\hat{\mathbf{s}}$ tilted with respect to the orbit plane precesses. We refer to the spinning object as a planet in orbit about a star, however we keep in mind that we can also consider a spinning satellite in orbit about a planet, asteroid or Kuiper belt object. We assume that the planet is rapidly spinning about its principal inertial axis and this is known as the *gyroscopic approximation*. The planet's moments of inertia are A, C with $A > C$ and the planet's spin angular momentum is $\mathbf{L}_s = wC\hat{\mathbf{s}}$ where w is the spin angular rotation rate and $\hat{\mathbf{s}}$ is a unit vector. The planet's spin axis satisfies

$$\frac{d\hat{\mathbf{s}}}{dt} = \alpha_s(\hat{\mathbf{s}}\cdot\hat{\mathbf{n}})(\hat{\mathbf{s}}\times\hat{\mathbf{n}}) \tag{2}$$

(Colombo 1966), with time derivatives taken with respect to the inertial frame. Here $\hat{\mathbf{n}}$ is a unit vector perpendicular to the orbit plane, aligned with the orbital angular momentum vector. The precession rate

$$\alpha_s = \frac{3}{2}\frac{(C-A)}{Cw}\frac{n^2}{(1-e^2)^{\frac{3}{2}}}, \tag{3}$$

where the orbital mean motion is n and the orbital eccentricity is e.

MacCullagh's formula gives the instantaneous torque on an oblate planet due to point mass M_*

$$\mathbf{T} = 3(C-A)\frac{GM_*}{r^3}(\hat{\mathbf{r}}\cdot\hat{\mathbf{s}})(\hat{\mathbf{r}}\times\hat{\mathbf{s}}) \tag{4}$$

where $\mathbf{r} = r\hat{\mathbf{r}}$ is the vector between the planet's center of mass and M_*. Equation 2 can be derived using MacCullagh's formula for the instantaneous torque by averaging over the orbit or computing $\langle\mathbf{T}\rangle = \frac{1}{P}\int \mathbf{T}dt$ where the orbital period is $P = 2\pi/n$, and assuming that the planet remains spinning nearly about its principal axis (Colombo 1966). Thus equation 2 is consistent with

$$\frac{d\hat{\mathbf{s}}}{dt} = \frac{1}{Cw}\langle\mathbf{T}\rangle. \tag{5}$$

Due to secular perturbations arising from other planets, the orbit normal $\hat{\mathbf{n}}$ can be a function of time (e.g., Colombo 1966; Ward 1975). A time dependent equation 2 has been used to study tidal evolution into Cassini states (Colombo 1966; Ward 1975) and obliquity evolution of Mars (Ward 1973, 1979; Bills 1990) and Saturn (Ward & Hamilton 2004). Phenomena discovered and explored include capture into spin-secular resonance states (Saturn; Ward & Hamilton 2004) and chaotic obliquity evolution (Mars; Touma & Wisdom 1993).

2.1 A Hamiltonian model for spin about a principal axis

Using angular spherical coordinates ϕ, θ in an inertial reference frame to specify the spin axis

$$\hat{\mathbf{s}} = (\cos\phi\sin\theta, \sin\phi\sin\theta, \cos\theta), \tag{6}$$

equation 2 can be written as a Hamiltonian dynamical system with canonical momentum p, conjugate to the precession angle ϕ

$$p = (1-\cos\theta). \tag{7}$$

The Hamiltonian

$$H_n(p,\phi) = -\frac{\alpha_s}{2}(\hat{\mathbf{s}}\cdot\hat{\mathbf{n}})^2 \tag{8}$$

with $\hat{\mathbf{s}}$ a function of p, ϕ, (Goldreich & Toomre 1969; Peale 1974). Hamilton's equations are

$$\dot{p} = -\frac{\partial H_n}{\partial \phi} \quad (9)$$

$$\dot{\phi} = \frac{\partial H_n}{\partial p} \quad (10)$$

and are equivalent to the equations of motion for the spin axis in equation 2.

The angle $\phi \in [0, 2\pi]$ describes spin precession. With orbit normal $\hat{\mathbf{n}}$ in the z direction, $\theta \in [0, \pi]$ is the planet's obliquity. The canonical momentum $p \in [0, 2]$ with $p = 0$ at $\theta = 0$. With the addition of a third angle describing body orientation about the spin axis, ϕ, θ are Euler angles.

Equation 2 resembles equation 4 but with $\mathbf{r}$ replacing $\hat{\mathbf{n}}$. Because $\mathbf{r}$ is independent of θ, ϕ the instantaneous spin vector (prior to averaging over the orbit) can also be described with a Hamiltonian system with

$$H(p, \phi) = \frac{3}{2}\frac{(C-A)}{Cw}\frac{GM}{r^3}(\hat{\mathbf{s}} \cdot \hat{\mathbf{r}})^2, \quad (11)$$

again with $\hat{\mathbf{s}}$ a function of p, ϕ. Hamilton's equations are equations of motion equivalent to

$$\frac{d\hat{\mathbf{s}}}{dt} = \frac{1}{Cw}\mathbf{T}. \quad (12)$$

When averaged over the orbit period this equation is consistent with equation 2. The Hamiltonian in equation 11 can be averaged by writing r and $\hat{\mathbf{r}}$ in terms the mean anomaly and mean longitude and taking the average over one or both of these angles. The gyroscopic approximation should be a good one as long as the orbital period is much larger than the spin rotation period. For rigorous derivations with averaging see Boué & Laskar (2006).

2.2 Precessional Constant with Satellites

An spinning oblate planet locks its satellites to its equator plane so that the system precesses as a unit (Goldreich 1965). The precession rate in equation 3 can be modified to take into account the satellites with

$$\alpha_s = \frac{3}{2}\frac{n^2}{w}\frac{J_2 + q_s}{\lambda_C + l_s}, \quad (13)$$

(Ward 1975; French et al. 1993; Ward & Hamilton 2004) but neglecting the orbital eccentricity. Here J_2 is the coefficient of the second zonal gravity harmonic (from the quadrupole moment) of the planet's gravitational potential field and $\lambda_C = C/mR^2$ is the planet's moment of inertia about its principal axis normalized to the product of planet mass and the square of the planet's equatorial radius. The parameter

$$l_s \equiv \sum_j \frac{m_j}{m}\left(\frac{a_j}{R}\right)^2 \frac{n_j}{w} \quad (14)$$

is the angular momentum of the satellite system normalized to mR^2w where m_j, a_j, n_j are the masses, semi-major axes (for the orbit about the planet) and mean motions of each satellite. The parameter

$$q_s \equiv \frac{1}{2}\sum_j \frac{m_j}{m}\left(\frac{a_j}{R}\right)^2 \frac{\sin(\theta - I_j)}{\sin\theta} \quad (15)$$

is the effective quadrupole coefficient of the satellite system with q_s/J_2 being the ratio of the solar torque on the satellites to that directly exerted on the planet. Here θ is the planet's obliquity and I_j the inclination of the j-th satellite with respect to the planet's equatorial plane. Without satellites $q_s = l_s = 0$ and with $J_2 = (C-A)/(mR^2)$ equation 13 reduces to equation 3.

2.3 A Perturbed Hamiltonian Model

We consider a spinning planet in orbit about a star at zero orbital inclination. When averaged over the orbit period and over the longitude of the ascending node the Hamiltonian describing the planet's spin (equation 8)

$$H_0(p, \phi) = -\frac{\alpha_s}{2}p(2-p) \quad (16)$$

and giving spin precession rate

$$\dot{\phi} = -\alpha_s \cos\theta \quad (17)$$

with α_s as given in equation 13.

We consider a Hamiltonian model in the form

$$H(p, \phi, t) = H_0(p) + H_1(p, \phi, t) \quad (18)$$

where H_1 is a time dependent perturbation.

MacCullagh's formula gives the torque on our spinning planet due to the perturbing planet with mass m_p. The torque dependent upon the radial vector between the two planets

$$\mathbf{T} = 3(C-A)\frac{Gm_p}{|\mathbf{r} - \mathbf{r_p}|^5}\left((\mathbf{r} - \mathbf{r}_p)\cdot\hat{\mathbf{s}}\right)\left((\mathbf{r} - \mathbf{r}_p)\times\hat{\mathbf{s}}\right), \quad (19)$$

where $\mathbf{r}$ is the radial vector to the spinning planet and $\mathbf{r}_p$ the radial vector to the perturbing planet. The associated Hamiltonian perturbation term is

$$H_1(p, \phi, t) = \frac{3(C-A)}{Cw}\frac{Gm_p}{|\mathbf{r} - \mathbf{r_p}|^5}\frac{\left((\mathbf{r} - \mathbf{r}_p)\cdot\hat{\mathbf{s}}\right)^2}{2} \quad (20)$$

and it is a time dependent perturbation. $H_1 \ll H_0$ because the mass of the perturbing planet is much less than the mass of a star; $m_p \ll M_*$.

We describe the orbits in terms orbital elements a, e, i, I, Ω, M which are semi-major axis, eccentricity, inclination, longitude of the ascending node, argument of pericenter and mean anomaly, respectively. We also use the mean longitude $\lambda = \Omega + \omega + M$ and the longitude of pericenter $\varpi = \Omega + \omega$. Our spinning and perturbing planets orbit a star with mass M_*.

We now depart from the notation used above with $\mathbf{r}, \mathbf{r}_p$ referring to spinning and perturbing planet, respectively. Orbital elements for the object with the larger semi-major axis will be referred to with a prime $(a', e', I', \Omega', M', \lambda', \varpi')$ and those with the smaller semi-major axis without a prime. The ratio of semi-major axes $\alpha \equiv a/a'$. With radial vectors $\mathbf{r}$ and $\mathbf{r}'$ for inner and outer orbiting mass, equation 20 for the spinning planet becomes

$$H_1(p, \phi, t) = 3\frac{(C-A)}{Cw}n^2\frac{m_p}{M_*}\frac{a_s^2}{|\mathbf{r} - \mathbf{r}'|^5}\frac{\left((\mathbf{r} - \mathbf{r}')\cdot\hat{\mathbf{s}}\right)^2}{2} \quad (21)$$

where a_s is the semi-major axis of the spinning object.

$$a_s \equiv \begin{cases} a' & \text{for external spinning body} \\ a & \text{for internal spinning body.} \end{cases} \quad (22)$$

When the spinning body is external, we mean that it is perturbed by the mass m_p that has orbit interior to our spinning body.

Taking into account a satellite system around the spinning planet

$$\frac{(C-A)}{C} \rightarrow \frac{(J_2+q_s)}{(\lambda_C+l_s)}$$

(comparing equation 3 with 13) and defining

$$\Delta \equiv |\mathbf{r}-\mathbf{r}'|, \tag{23}$$

we can write equation 21 as

$$H_1(p,\phi,t) = \alpha_s \frac{m_p}{M_*}\left(\frac{a_s}{a'}\right)^3 \frac{a'^3}{\Delta^5}\left((\mathbf{r}-\mathbf{r}')\cdot\hat{\mathbf{s}}\right). \tag{24}$$

It is convenient to write time in terms of the precession constant with unitless $\tau = \alpha_s t$. The total Hamiltonian including perturbation (using equations 18, 16, 24)

$$H(p,\phi,\tau) = -\frac{p}{2}(2-p) + \beta\frac{a'^3}{\Delta^5}\left((\mathbf{r}-\mathbf{r}')\cdot\hat{\mathbf{s}}\right)^2 \tag{25}$$

with unitless coefficient

$$\beta \equiv \frac{m_p}{M_*}\left(\frac{a_s}{a'}\right)^3 \tag{26}$$

primarily dependent on the ratio m_p/M_* of perturbing planet and stellar masses.

2.4 Evaluating the perturbation term in the Hamiltonian to first order in inclination

From the Hamiltonian in equation 25 we evaluate

$$\frac{a'^3}{\Delta^5} \qquad \text{and} \qquad \left((\mathbf{r}-\mathbf{r}')\cdot\hat{\mathbf{s}}\right)^2,$$

keeping terms that are zero-th order in orbital eccentricity and first order in inclination. With radial vector $\mathbf{r} = (x,y,z)$, in terms of orbital elements

$$\mathbf{r} = r\begin{pmatrix} \cos\Omega\cos(\omega+f) - \sin\Omega\sin(\omega+f)\cos I \\ \sin\Omega\cos(\omega+f) + \cos\Omega\sin(\omega+f)\cos I \\ \sin(\omega+f)\sin I \end{pmatrix}, \tag{27}$$

and likewise for the other mass at $\mathbf{r}'$ using primed orbital elements. To zero-th order in eccentricity (or for $e=0$) we can replace the true anomaly f with the mean anomaly M in the above expression. As is customary at low inclination (Murray & Dermott 1999) we let

$$\cos I \approx 1 - I^2/2 \approx 1 - 2s^2$$
$$\sin I \approx I \approx 2s.$$

To zero-th order in e but first order in s equation 27 can be written as

$$\frac{x}{r} \approx \frac{x}{a} \approx \cos(\omega+\Omega+M) \approx \cos\lambda$$
$$\frac{y}{r} \approx \frac{y}{a} \approx \sin(\omega+\Omega+M) \approx \sin\lambda$$
$$\frac{z}{r} \approx \frac{z}{a} \approx 2s\sin(\omega+M) \approx 2s\sin(\lambda-\Omega). \tag{28}$$

We compute the dot product of $\mathbf{r}$ with the spin vector $\hat{\mathbf{s}}$ as given in equation 6 to first order in inclination variable s

$$\frac{\mathbf{r}\cdot\hat{\mathbf{s}}}{a} \approx \sin\theta\cos(\lambda-\phi) + \cos\theta(2s)\sin(\lambda-\Omega), \tag{29}$$

and

$$\frac{(\mathbf{r}\cdot\hat{\mathbf{s}})^2}{a^2} \approx \frac{\sin^2\theta}{2}\left[1+\cos(2(\lambda-\phi))\right] + 2s\sin\theta\cos\theta\left[\sin(2\lambda-\Omega-\phi) + \sin(\phi-\Omega)\right]. \tag{30}$$

One can average over the orbital period by integrating this square over 2π in mean longitude λ. The terms proportional to $\cos(2(\lambda-\phi))$ and $\sin(2\lambda-\Omega-\phi)$ average to zero. The secular term proportional to $\sin(\phi-\Omega)$ only disappears if an additional average over Ω or ϕ is performed. This leaves only $\sin^2\theta/2$, consistent with the Hamiltonians in equations 8 and 16.

The cross term in $((\mathbf{r}-\mathbf{r}')\cdot\hat{\mathbf{s}})^2$

$$\begin{aligned}\frac{(\mathbf{r}\cdot\hat{\mathbf{s}})(\mathbf{r}'\cdot\hat{\mathbf{s}})}{aa'} \approx{}& \frac{\sin^2\theta}{2}\left[\cos(\lambda+\lambda'-2\phi)+\cos(\lambda-\lambda')\right] \\ &+ \sin\theta\cos\theta s\left[\sin(\lambda+\lambda'-\Omega-\phi) + \sin(\lambda-\lambda'-\Omega+\phi)\right] \\ &+ \sin\theta\cos\theta s'\left[\sin(\lambda+\lambda'-\Omega'-\phi) - \sin(\lambda-\lambda'-\Omega'+\phi)\right].\end{aligned} \tag{31}$$

In celestial mechanics the *disturbing function*, arising from gravitational interactions between point masses, contains

$$\frac{1}{\Delta} = \frac{1}{|\mathbf{r}-\mathbf{r}'|} = (r^2+r'^2-2rr'\cos\psi)^{-\frac{1}{2}}$$

with $\cos\psi \equiv (\hat{\mathbf{r}}\cdot\hat{\mathbf{r}}')$. As is common in expansions of the disturbing function we define

$$\Psi \equiv \cos\psi - \cos(\varpi+f-\varpi'-f') \tag{32}$$

$$\Delta_0 \equiv \left[r^2+r'^2-2rr'\cos(\varpi+f-\varpi'-f')\right]^{-\frac{1}{2}} \tag{33}$$

giving

$$\Delta^{-1} = \left[r^2+r'^2-2rr'(\cos(\varpi+f-\varpi'-f')+\Psi)\right]^{-\frac{1}{2}} \tag{34}$$

(see page 235 by Murray & Dermott 1999). To first order in Ψ,

$$\Delta^{-1} \approx \Delta_0^{-1} + rr'\Delta_0^{-3}\Psi. \tag{35}$$

Likewise to first order in Ψ,

$$\Delta^{-5} \approx \Delta_0^{-5} + 5rr'\Delta_0^{-7}\Psi. \tag{36}$$

Our Hamiltonian term depends on Δ^{-5} rather than the inverse of Δ as is true for the disturbing function. To second order in inclinations

$$\begin{aligned}\Psi \approx{}& s^2\left(\cos(\lambda+\lambda'-2\Omega)-\cos(\lambda-\lambda')\right) \\ &+ ss'\left(\cos(\lambda-\lambda'-\Omega+\Omega')-\cos(\lambda+\lambda'-\Omega-\Omega')\right) \\ &+ s'^2\left(\cos(\lambda+\lambda'-2\Omega')-\cos(\lambda-\lambda')\right)\end{aligned} \tag{37}$$

(see Murray & Dermott 1999 page 240). As Ψ lacks zeroth and first order terms in inclination, we need only take the first term in equation 36 to carry out an expansion to first order in inclination. Expanding Δ_0

$$\Delta_0^{-(2i+1)} = \frac{1}{2}\sum_{j=-\infty}^{\infty}\cos[j(\varpi+f-\varpi'-f')]\times \left[\sum_{l=0}^{\infty}\frac{1}{l!}\sum_{k=0}^{l}\binom{l}{k}\left(\frac{r}{a}-1\right)^k\left(\frac{r'}{a'}-1\right)^{l-k}A_{i,j,k,l-k}\right] \tag{38}$$

(see equation 6.65 by Murray & Dermott 1999) with coefficients

$$A_{i,j,m,n}(\alpha) \equiv a^m a'^n \frac{\partial^{m+n}}{\partial a^m \partial a'^n}\left(a'^{-(2i+1)} b^{(j)}_{i+\frac{1}{2}}(\alpha)\right), \quad (39)$$

where $b^{(j)}_s(\alpha)$ is a Laplace coefficient dependent on the ratio of semi-major axes $\alpha = a/a' < 1$.

To zero-th order in eccentricities ($e = e' = 0$) we need only evaluate

$$A_{2,j,0,0}(\alpha) = \frac{1}{a'^5} b^{(j)}_{5/2}(\alpha), \quad (40)$$

giving to first order in inclination (and with $e = e' = 0$)

$$\Delta^{-5} \approx \Delta_0^{-5} \approx \frac{1}{2a'^5} \sum_{j=-\infty}^{\infty} \cos[j(\lambda - \lambda')] b^{(j)}_{5/2}(\alpha). \quad (41)$$

Using equations 30, 31 and 41 to zero-th order in eccentricity and first order in inclination

$$\begin{aligned}
&\frac{a'^3}{\Delta^5}((\mathbf{r} - \mathbf{r}') \cdot \hat{\mathbf{s}})^2 \approx \\
&\quad \Bigg\{ \frac{\sin^2\theta}{2}\Big[1 + \alpha^2 \\
&\qquad + \alpha^2 \cos(2(\lambda - \phi)) + \cos(2(\lambda' - \phi)) \\
&\qquad - 2\alpha\cos(\lambda + \lambda' - 2\phi) - 2\alpha\cos(\lambda - \lambda')\Big] \\
&\quad + 2\sin\theta\cos\theta \times \Big[\\
&\qquad s\alpha^2 \sin(2\lambda - \Omega - \phi) + s\alpha^2 \sin(\phi - \Omega) \\
&\qquad + s' \sin(2\lambda' - \Omega' - \phi) + s' \sin(\phi - \Omega') \\
&\qquad - s\alpha \sin(\lambda + \lambda' - \Omega - \phi) \\
&\qquad - s\alpha \sin(\lambda - \lambda' - \Omega + \phi) \\
&\qquad - s'\alpha \sin(\lambda + \lambda' - \Omega' - \phi) \\
&\qquad + s'\alpha \sin(\lambda - \lambda' - \Omega' + \phi)\Big] \Bigg\} \\
&\qquad \times \frac{1}{2} \sum_{j=-\infty}^{\infty} b^{(j)}_{5/2}(\alpha) \cos(j(\lambda - \lambda')). \quad (42)
\end{aligned}$$

The non-secular terms with arguments that are not multiples of $\lambda - \lambda'$ can be rewritten in terms of a single cosine or sine of orbital elements and ϕ;

$$\begin{aligned}
&\frac{\sin^2\theta}{8}\Big[\cos(j\lambda - (j-2)\lambda' - 2\phi)\left(\alpha^2 b^{(j-2)}_{5/2} + b^{(j)}_{5/2} - 2\alpha b^{(j-1)}_{5/2}\right) \\
&\quad + \cos(j\lambda - (j+2)\lambda' + 2\phi)\left(\alpha^2 b^{(j+2)}_{5/2} + b^{(j)}_{5/2} - 2\alpha b^{(j+1)}_{5/2}\right)\Big] \\
&+ \frac{\sin\theta\cos\theta}{2} \times \Big[\\
&\quad \sin(j\lambda - (j-2)\lambda' - \Omega' - \phi)(b^{(j)}_{5/2} - \alpha b^{(j-1)}_{5/2})s' \\
&\quad - \sin(j\lambda - (j+2)\lambda' + \Omega' + \phi)(b^{(j)}_{5/2} - \alpha b^{(j+1)}_{5/2})s' \\
&\quad + \sin(j\lambda - (j-2)\lambda' - \Omega - \phi)(\alpha^2 b^{(j-2)}_{5/2} - \alpha b^{(j-1)}_{5/2})s \\
&\quad - \sin(j\lambda - (j+2)\lambda' + \Omega + \phi)(\alpha^2 b^{(j+2)}_{5/2} - \alpha b^{(j+1)}_{5/2})s\Big]. \quad (43)
\end{aligned}$$

Arguments that are rapidly varying will not strongly perturb the spinning planet as they effectively average to zero. Only slowly varying arguments give resonantly strong perturbations. The external body has a slower mean motion than the internal one; $n' < n$ recalling that $n = \dot{\lambda}$. The slow arguments must be those containing $\lambda - (j+2)\lambda'$ and so are associated with second order mean motion resonances. Retaining only those three arguments in equation 43 for a single j and using equations 42 and 43 we can write a near resonance Hamiltonian (equation 25) as

$$\begin{aligned}
H(p,\phi,\tau)^{j:j+2} &= -\frac{p}{2}(2-p) \\
&\quad + \beta c_0^j p(2-p)\cos(j\lambda - (j+2)\lambda' + 2\phi) \\
&\quad + (1-p)\sqrt{p(2-p)}\times \\
&\qquad \Big[\beta c_s^j s \sin(j\lambda - (j+2)\lambda' + \Omega + \phi) \\
&\qquad\quad + \beta c_{s'}^j s' \sin(j\lambda - (j+2)\lambda' + \Omega' + \phi)\Big], \quad (44)
\end{aligned}$$

where we have replaced θ with p using $\sin\theta\cos\theta = (1-p)\sqrt{p(2-p)}$ and $\sin^2\theta = p(2-p)$. The unitless coefficients

$$\begin{aligned}
c_0^j(\alpha) &\equiv \frac{1}{4}\left(\alpha^2 b^{(j+2)}_{5/2}(\alpha) + b^{(j)}_{5/2}(\alpha) - 2\alpha b^{(j+1)}_{5/2}(\alpha)\right) \\
c_s^j(\alpha) &\equiv \left(\alpha b^{(j+1)}_{5/2}(\alpha) - \alpha^2 b^{(j+2)}_{5/2}(\alpha)\right) \\
c_{s'}^j(\alpha) &\equiv \left(\alpha b^{(j+1)}_{5/2}(\alpha) - b^{(j)}_{5/2}(\alpha)\right). \quad (45)
\end{aligned}$$

These coefficients are twice those in equation 43 because we have taken positive and negative j terms that give the same argument. We recall that time is in units of α_s as defined in equation 13 and the coefficient β depends on the mass ratio m_p/M_* (equation 26). To aid in applications we have computed these coefficients for $j = 1$ to 6 and their values are listed in Table 2.

Our Hamiltonian (equation 44) contains terms that are first order in orbital inclination. This is to be compared to first order mean motion orbital resonances that lack first order terms (in s) in an expansion of the disturbing function and second order inclination mean motion resonances that by definition are proportional to s^2. Previous calculations of spin perturbations have considered the role of secular frequencies on planet spin orientation by considering how the orbit variations affect the torque from the star. In contrast here we have directly evaluated the torque from a nearby planet.

We could similarly consider how a nearby planet induces perturbations on the orbit of our spinning planet and then expand the equation for the torque from the star taking into account these perturbations. The orbit perturbations arising from the perturbing planet depends on the ratio of m_p/M_* as does our β, but here our Hamiltonian perturbation contains both zeroth and first order terms in s. In contrast near a second order resonance orbital perturbations are likely to be second order in e and s. Because it contains zeroth and first order terms in the expansion, the torque directly exerted onto the spinning planet from a nearby planet might be stronger than variations on the torque from the star caused by orbital perturbations from a perturbing planet. We have neglected these orbital perturbations, but future work could take them into account.

In our numerical exploration of Styx we found two slowly moving angles, ϕ_{s1}, ϕ_{s2} (defined in equation 1) when there were obliquity variations. These angles can be recognized as arguments in the Hamiltonian in equation 44 with index $j = 1$, and identifying $\lambda' = \lambda_{Styx}$ and $\lambda = \lambda_{Charon}$. Our perturbation computation gives terms with arguments

Table 2. Resonance coefficients

Resonance	j	α	$c_0^j(\alpha)$	$c_s^j(\alpha)$	$c_{s'}^j(\alpha)$
3:1	1	0.481	0.765	1.782	-4.844
4:2	2	0.630	1.312	6.173	-11.423
5:3	3	0.711	2.027	14.270	-22.378
6:4	4	0.763	2.904	27.179	-38.793
7:5	5	0.799	3.941	45.999	-61.763
8:6	6	0.825	5.139	71.831	-92.386
Resonance	j	α	$c_{e1}^j(\alpha)$	$c_{e'1}^j(\alpha)$	
2:1	1	0.630	-26.751	-0.384	
3:2	2	0.763	-168.337	-0.179	
4:3	3	0.825	-584.812	0.799	
5:4	4	0.862	-1505.813	2.943	
6:5	5	0.886	-3231.011	6.647	
7:6	6	0.902	-6130.115	12.304	
Resonance	j	α	$c_{e3}^j(\alpha)$	$c_{e'3}^j(\alpha)$	
4:1	1	0.397	-1.238	2.997	
5:2	2	0.543	-3.255	5.831	
6:3	3	0.630	-6.546	10.170	
7:4	4	0.689	-11.425	16.304	
8:5	5	0.731	-18.201	24.534	

These are coefficients defined in equations 45, 58, and 59. We used series expansions for the Laplace coefficients to compute them.

consistent with the form we guessed from the slow moving angles we had seen in our simulations (see Quillen et al. 2017). Our Hamiltonian model effectively describes those spin-resonances.

2.5 Perturbation terms to first order in eccentricity

From the Hamiltonian in equation 25 we evaluate

$$\frac{a'^3}{\Delta^5} \qquad \text{and} \qquad \left((\mathbf{r}-\mathbf{r}')\cdot\hat{\mathbf{s}}\right)^2,$$

but keeping terms that are first order in orbital eccentricity and zeroth-order in inclination. To first order in orbital eccentricity e equation 28 gains these terms

$$\begin{aligned}\frac{x}{a} &\stackrel{+}{=} e(\frac{1}{2}\cos(2\lambda-\varpi)-\frac{3}{2}\cos\varpi)\\ \frac{y}{a} &\stackrel{+}{=} e(\frac{1}{2}\sin(2\lambda-\varpi)-\frac{3}{2}\sin\varpi))\\ \frac{z}{a} &\stackrel{+}{=} 0.\end{aligned} \tag{46}$$

We have neglected terms that are proportional to es. Equation 29 gains these terms

$$\frac{\mathbf{r}\cdot\hat{\mathbf{s}}}{a} \stackrel{+}{=} \frac{e}{2}\sin\theta\big[\cos(2\lambda-\varpi-\phi)-3\cos(\varpi-\phi)\big]. \tag{47}$$

Equation 30 gains

$$\begin{aligned}\frac{(\mathbf{r}\cdot\hat{\mathbf{s}})^2}{a^2} \stackrel{+}{=} e\frac{\sin^2\theta}{2}\Big[&\cos(3\lambda-\varpi-2\phi)\\ &-3\cos(\lambda+\varpi-2\phi)-2\cos(\lambda-\varpi)\Big].\end{aligned} \tag{48}$$

Equation 31 gains

$$\begin{aligned}\frac{(\mathbf{r}\cdot\hat{\mathbf{s}})(\mathbf{r}'\cdot\hat{\mathbf{s}})}{aa'} \stackrel{+}{=} \frac{\sin^2\theta}{4}\Big\{&\\ &e\Big[\cos(2\lambda+\lambda'-\varpi-2\phi)+\cos(2\lambda-\lambda'-\varpi)\\ &-3\cos(\lambda'+\varpi-2\phi)-3\cos(\lambda'-\varpi)\Big]+\\ &e'\Big[\cos(2\lambda'+\lambda-\varpi'-2\phi)+\cos(2\lambda'-\lambda-\varpi')\\ &-3\cos(\lambda+\varpi'-2\phi)-3\cos(\lambda-\varpi')\Big]\Big\}.\end{aligned} \tag{49}$$

Using

$$\frac{\partial}{\partial a}=\frac{1}{a'}D_\alpha \qquad \text{and} \qquad \frac{\partial}{\partial a'}=-\frac{\alpha}{a'}D_\alpha \tag{50}$$

for derivatives, with $D_\alpha \equiv \frac{d}{d\alpha}$, we compute coefficients (as defined in equation 39)

$$\begin{aligned}A_{2,j,0,1} &= a'^{-5}\left[-5b_{5/2}^{(j)}(\alpha)+a'\frac{\partial}{\partial a'}b_{5/2}^{(j)}(\alpha)\right]\\ &= -\frac{1}{a'^5}[5+\alpha D_\alpha]b_{5/2}^{(j)}(\alpha)\\ A_{2,j,1,0} &= a'^{-5}a\frac{\partial}{\partial a}b_{5/2}^{(j)}(\alpha)=\frac{1}{a'^5}\alpha D_\alpha b_{5/2}^{(j)}(\alpha).\end{aligned} \tag{51}$$

To first order in e, e'

$$\begin{aligned}\cos[j(\varpi+f-\varpi'-f')] \approx &\cos[j(\lambda-\lambda')]\\ &+je\cos[(1+j)\lambda-j\lambda'-\varpi)]\\ &-je\cos[(1-j)\lambda+j\lambda'-\varpi)]\\ &-je'\cos[j\lambda+(1-j)\lambda'-\varpi')]\\ &+je'\cos[j\lambda-(1+j)\lambda'+\varpi')]\end{aligned} \tag{52}$$

using equation 6.90 by Murray & Dermott (1999).

Taking first order terms from equation 52, the coefficients 51 and noting that in equation 38 the factor $\left(\frac{r}{a}-1\right)\approx -e\cos M = -e\cos(\lambda-\varpi)$ to first order in e, we can compute first order (in eccentricity) terms from equation 38

$$\begin{aligned}\Delta_0^{-5} \stackrel{+}{=} \frac{1}{2a'^5}\sum_{j=-\infty}^{\infty}\Bigg\{&\\ &e\Bigg[\cos[(j+1)\lambda-j\lambda'-\varpi]\left(-\frac{\alpha}{2}D_\alpha+j\right)b_{5/2}^{(j)}(\alpha)\\ &+\cos[(j-1)\lambda-j\lambda'+\varpi]\left(-\frac{\alpha}{2}D_\alpha-j\right)b_{5/2}^{(j)}(\alpha)\Big)\Bigg]+\\ &e'\Bigg[\cos[j\lambda-(j-1)\lambda'-\varpi']\left(\frac{\alpha}{2}D_\alpha+\frac{5}{2}-j\right)b_{5/2}^{(j)}(\alpha)\\ &+\cos[j\lambda-(j+1)\lambda'+\varpi']\left(\frac{\alpha}{2}D_\alpha+\frac{5}{2}+j\right)b_{5/2}^{(j)}(\alpha)\Big)\Bigg]\Bigg\}.\end{aligned} \tag{53}$$

These terms are added to equation 41 giving Δ^{-5} to first order in e, e'.

Using equations 30, 31, 41, 48, 49, and 53 we compute the first order in eccentricity terms that are added to equation 42;

$$\begin{aligned}
&\frac{a'^3((\mathbf{r}-\mathbf{r}')\cdot\hat{\mathbf{s}})^2}{\Delta^5} \overset{+}{\approx} \frac{\sin^2\theta}{4}\Bigg\{ \\
&\quad e\alpha^2\Big[\cos(3\lambda-\varpi-2\phi) \\
&\qquad -3\cos(\lambda+\varpi-2\phi)-2\cos(\lambda-\varpi)\Big] \\
&\quad -e\alpha\Big[\cos(2\lambda+\lambda'-\varpi-2\phi)+\cos(2\lambda-\lambda'-\varpi) \\
&\qquad -3\cos(\lambda'+\varpi-2\phi)-3\cos(\lambda'-\varpi)\Big] \\
&\quad -e'\alpha\Big[\cos(2\lambda'+\lambda-\varpi'-2\phi)+\cos(2\lambda'-\lambda-\varpi') \\
&\qquad -3\cos(\lambda+\varpi'-2\phi)-3\cos(\lambda-\varpi')\Big] \\
&\quad +e'\Big[\cos(3\lambda'-\varpi'-2\phi) \\
&\qquad -3\cos(\lambda'+\varpi'-2\phi)-2\cos(\lambda'-\varpi')\Big] \\
&\quad \times\sum_{j=-\infty}^{\infty} b_{5/2}^{(j)}(\alpha)\cos(j\lambda-j\lambda')\ldots \\
&\quad +\Big(1+\alpha^2+\alpha^2\cos(2\lambda-2\phi)+\cos(2\lambda'-2\phi) \\
&\quad -2\alpha\cos(\lambda+\lambda'-2\phi)-2\alpha\cos(\lambda-\lambda')\Big) \\
&\quad \times\sum_{j=-\infty}^{\infty}\Bigg[\\
&\qquad e\cos[(j+1)\lambda-j\lambda'-\varpi]\left(-\frac{\alpha}{2}D_\alpha+j\right)b_{5/2}^{(j)}(\alpha) \\
&\qquad +e\cos[(j-1)\lambda-j\lambda'+\varpi]\left(-\frac{\alpha}{2}D_\alpha-j\right)b_{5/2}^{(j)}(\alpha)+ \\
&\qquad +e'\cos[j\lambda+(1-j)\lambda'-\varpi']\left(\frac{\alpha}{2}D_\alpha+\frac{5}{2}-j\right)b_{5/2}^{(j)}(\alpha) \\
&\qquad +e'\cos[j\lambda-(1+j)\lambda'+\varpi']\left(\frac{\alpha}{2}D_\alpha+\frac{5}{2}+j\right)b_{5/2}^{(j)}(\alpha)\Bigg]\Bigg\}
\end{aligned} \tag{54}$$

Combining arguments and taking only arguments that contain ϕ these terms can be written

$$\begin{aligned}
&\cos[j\lambda-(j-3)\lambda'-\varpi-2\phi] && \frac{\sin^2\theta}{8}e\Big[\alpha^2\left(-\frac{\alpha}{2}D_\alpha+j-2\right)b_{5/2}^{(j-3)}+\alpha\left(\alpha D_\alpha-2j+3\right)b_{5/2}^{(j-2)}+\left(-\frac{\alpha}{2}D_\alpha+j-1\right)b_{5/2}^{(j-1)}\Big]+ \\
&\cos[j\lambda-(j+3)\lambda'+\varpi+2\phi] && \frac{\sin^2\theta}{8}e\Big[\alpha^2\left(-\frac{\alpha}{2}D_\alpha-j-2\right)b_{5/2}^{(j+3)}+\alpha\left(\alpha D_\alpha+2j+3\right)b_{5/2}^{(j+2)}+\left(-\frac{\alpha}{2}D_\alpha-j-1\right)b_{5/2}^{(j+1)}\Big]+ \\
&\cos[j\lambda-(j-3)\lambda'-\varpi'-2\phi] && \frac{\sin^2\theta}{8}e'\Big[\alpha^2\left(\frac{\alpha}{2}D_\alpha-j+\frac{9}{2}\right)b_{5/2}^{(j-2)}+\alpha\left(-\alpha D_\alpha+2j-8\right)b_{5/2}^{(j-1)}+\left(\frac{\alpha}{2}D_\alpha-j+\frac{7}{2}\right)b_{5/2}^{(j)}\Big]+ \\
&\cos[j\lambda-(j+3)\lambda'+\varpi'+2\phi] && \frac{\sin^2\theta}{8}e'\Big[\alpha^2\left(\frac{\alpha}{2}D_\alpha+j+\frac{9}{2}\right)b_{5/2}^{(j+2)}+\alpha\left(-\alpha D_\alpha-2j-8\right)b_{5/2}^{(j+1)}+\left(\frac{\alpha}{2}D_\alpha+j+\frac{7}{2}\right)b_{5/2}^{(j)}\Big]+ \\
&\cos[j\lambda-(j-1)\lambda'+\varpi-2\phi] && \frac{\sin^2\theta}{8}e\Big[\left(-\frac{\alpha}{2}D_\alpha-j-1\right)b_{5/2}^{(j+1)}+\alpha\left(\alpha D_\alpha+2j-3\right)b_{5/2}^{(j)}+\alpha^2\left(-\frac{\alpha}{2}D_\alpha-j-2\right)b_{5/2}^{(j-1)}\Big]+ \\
&\cos[j\lambda-(j+1)\lambda'-\varpi+2\phi] && \frac{\sin^2\theta}{8}e\Big[\alpha^2\left(-\frac{\alpha}{2}D_\alpha+j-2\right)b_{5/2}^{(j+1)}+\alpha\left(\alpha D_\alpha-2j-3\right)b_{5/2}^{(j)}+\left(-\frac{\alpha}{2}D_\alpha+j-1\right)b_{5/2}^{(j-1)}\Big]+ \\
&\cos[j\lambda-(j-1)\lambda'-\varpi'+2\phi] && \frac{\sin^2\theta}{8}e'\Big[\alpha^2\left(\frac{\alpha}{2}D_\alpha+j+\frac{1}{2}\right)b_{5/2}^{(j-2)}+\alpha\left(-\alpha D_\alpha-2j\right)b_{5/2}^{(j-1)}+\left(\frac{\alpha}{2}D_\alpha+j-\frac{1}{2}\right)b_{5/2}^{(j)}\Big]+ \\
&\cos[j\lambda-(j+1)\lambda'+\varpi'-2\phi] && \frac{\sin^2\theta}{8}e'\Big[\alpha^2\left(\frac{\alpha}{2}D_\alpha-j+\frac{1}{2}\right)b_{5/2}^{(j+2)}+\alpha\left(-\alpha D_\alpha+2j\right)b_{5/2}^{(j+1)}+\left(\frac{\alpha}{2}D_\alpha-j-\frac{1}{2}\right)b_{5/2}^{(j)}\Big]
\end{aligned} \tag{55}$$

Inspection of the arguments in equation 55 implies that resonant terms will be important (with slowly varying arguments) near first order mean motion resonances, where $j\lambda-(j+1)\lambda'$ is slowly varying (with positive j) and near third order mean motion resonances, where $j\lambda-(j+3)\lambda'$) is slowly varying. Near a third order mean motion resonance (and to first order in eccentricities and inclinations) we can consider a near resonance Hamiltonian (similar to equation 44)

$$\begin{aligned}
H(p,\phi,\tau)^{j:j+3} \approx &-\frac{p}{2}(2-p)+ \\
&\beta c_{e3}^{j} ep(2-p)\cos[j\lambda-(j+3)\lambda'+\varpi+2\phi]+ \\
&\beta c_{e'3}^{j} e'p(2-p)\cos[j\lambda-(j+3)\lambda'+\varpi'+2\phi].
\end{aligned} \tag{56}$$

Near a third order mean motion resonance, we can neglect the terms we previously computed (zero-th order in e, e' and first order in s, s') because they are only important near second order mean motion resonances. However, at higher order in e, e', s, s' additional terms will contribute near all of these mean motion resonances.

Near a third order mean motion resonance, equation 56 shows that the torque directly exerted by the planet is first order in eccentricity. The perturbing planet should cause orbital perturbations depending upon the third order of the eccentricity. So the variations in the torque from the star due to the orbit variations are likely to be smaller than the those caused directly from the torque of the perturbing planet.

Near a first order mean motion resonance

$$H(p,\phi,\tau)^{j:j+1} \approx -\frac{p}{2}(2-p)+$$
$$\beta c_0^{2j}\frac{p}{2}(2-p)\cos[2(\lambda-(j+1)\lambda')+2\phi]+$$
$$\beta c_s^{2j}s(1-p)\sqrt{p(2-p)}\sin[2(\lambda-(j+1)\lambda')+\Omega+\phi]+$$
$$\beta c_{s'}^{2j}s'(1-p)\sqrt{p(2-p)}\sin[2(\lambda-(j+1)\lambda')+\Omega'+\phi]+$$
$$\beta c_{e1}^{j}e\frac{p}{2}(2-p)\cos[j\lambda-(j+1)\lambda'-\varpi+2\phi]+$$
$$\beta c_{e'1}^{j}e'\frac{p}{2}(2-p)\cos[j\lambda-(j+1)\lambda'-\varpi'+2\phi]. \quad (57)$$

Here zero-th order and first order in inclination terms contribute but they are indexed by $2j$ rather than j.

Near a first order mean motion resonance, equation 57 shows that the torque directly exerted by the planet is first order in eccentricity. The perturbing planet would also cause orbital perturbations that are first order in eccentricity. Variations in the torque from the star due to the orbit variations could be similar in size to those caused directly from the torque of the perturbing planet and these could be computed in future work.

The coefficients for Hamiltonians in equation 56 and 57 are twice those listed in equation 55 so as to include the contribution from a corresponding negative j term that gives the same argument;

$$c_{e3}^{j} \equiv \frac{1}{4}\left[\alpha^2\left(-\frac{\alpha}{2}D_\alpha-j-2\right)b_{5/2}^{(j+3)}+\right.$$
$$\left.\alpha\left(\alpha D_\alpha+2j+3\right)b_{5/2}^{(j+2)}+\left(-\frac{\alpha}{2}D_\alpha-j-1\right)b_{5/2}^{(j+1)}\right]$$
$$c_{e'3}^{j} \equiv \frac{1}{4}\left[\alpha^2\left(\frac{\alpha}{2}D_\alpha+j+\frac{9}{2}\right)b_{5/2}^{(j+2)}+\right.$$
$$\left.\alpha\left(-\alpha D_\alpha-2j-8\right)b_{5/2}^{(j+1)}+\left(\frac{\alpha}{2}D_\alpha+j+\frac{7}{2}\right)b_{5/2}^{(j)}\right] \quad (58)$$

and

$$c_{e1}^{j} \equiv \frac{1}{4}\left[\alpha^2\left(-\frac{\alpha}{2}D_\alpha+j-2\right)b_{5/2}^{(j+1)}+\right.$$
$$\left.\alpha\left(\alpha D_\alpha-2j-3\right)b_{5/2}^{(j)}+\left(-\frac{\alpha}{2}D_\alpha+j-1\right)b_{5/2}^{(j-1)}\right]$$
$$c_{e'1}^{j} \equiv \frac{1}{4}\left[\alpha^2\left(\frac{\alpha}{2}D_\alpha-j+\frac{1}{2}\right)b_{5/2}^{(j+2)}+\right.$$
$$\left.\alpha\left(-\alpha D_\alpha+2j\right)b_{5/2}^{(j+1)}+\left(\frac{\alpha}{2}D_\alpha-j-\frac{1}{2}\right)b_{5/2}^{(j)}\right]. \quad (59)$$

For low j we computed these coefficients and list them in Table 2.

Near a second order mean motion resonance $(j:j+2)$ with j an odd integer, the first order in eccentricity terms do not contribute. Consequently equation 44 remains accurate to first order in eccentricity for odd j second order mean motion resonances.

3 DRIFTING TOY HAMILTONIAN MODELS

The perturbations to the Hamiltonian arising from terms that are zero-th order in inclination and eccentricity are proportional to $\sin^2\theta$ (see equation 43). These would be important near first and second order mean motion resonances, as shown in the Hamiltonians in equations 44 and 57. Perturbations that are first order in eccentricity are also proportional to $\sin^2\theta$ (see equation 55) and these would be important near first and third order mean motion resonances (as in the Hamiltonians given in equation 56 and 57). In contrast perturbations that are first order in inclination are proportional to $\sin\theta\cos\theta$ (see equation 43). These are relevant for first and second order mean motion resonances (as in the Hamiltonians given in equations 44 and 57). We have two types of perturbations, those proportional to $\sin^2\theta$ and those proportional to $\sin\theta\cos\theta$. In terms of p, the canonical momentum, $\sin^2\theta = p(2-p)$ and $\sin\theta\cos\theta = (1-p)\sqrt{p(2-p)}$. The two types of perturbation terms give Hamiltonians with different shapes (as a function of p) and this affects the resonance strength as a function of obliquity.

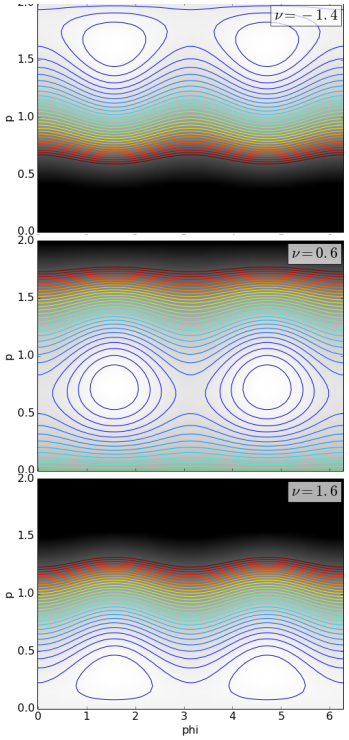

Figure 1. Level contours of the Hamiltonian in equation 64 with a perturbation proportional to $\sin^2\theta$ with resonance strength $\beta c_0^j = 0.05$. Each subplot shows level contours of the Hamiltonian with a different value of distance to resonance ν_2 and with the value of ν_2 labelled on the upper right. For $|\nu_2|<2$ there are two stable and two unstable fixed points. For $|\nu_2|\geqslant 2$ there are no fixed points.

3.1 Hamiltonian model for a perturbation proportional to $\sin^2\theta$

Taking the Hamiltonian in equation 44, appropriate for a second order mean motion resonance we define a frequency

$$\nu_2 \equiv \alpha_s^{-1}(jn-(j+2)n'). \quad (60)$$

Here the spin precession frequency α_s makes ν_2 unitless. Retaining a single j term and zero-th order (in inclination)

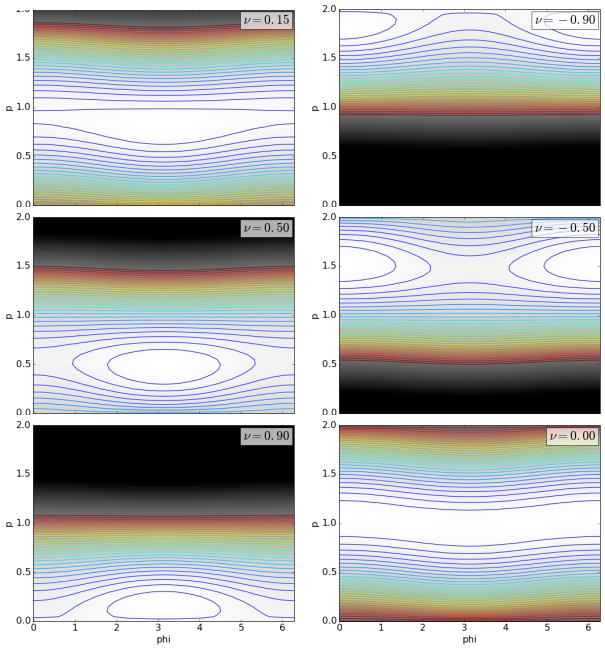

Figure 2. Level contours of the Hamiltonian in equation 70 with a term first order in inclination proportional to $\sin\theta\cos\theta$, with resonance strength $\beta c_s^j s = 0.05$ and for different values of distance to resonance ν_2. This Figure is similar to Figure 1. For $0 < \nu_2 < 1$ there is a single stable fixed point at $\varphi = \pi$. For $-1 < \nu_2 < 0$ there is a single stable fixed point at $\varphi = 0$. For $|\nu_2| \geqslant 1$ and $\nu_2 = 0$ there are no fixed points.

perturbation term alone the Hamiltonian in equation 44

$$H(p,\phi,\tau)_{c0j} = -\frac{p}{2}(2-p) + \beta c_0^j p(2-p)\cos(\nu_2\tau + 2\phi + c) \quad (61)$$

with c a constant phase.

A similar Hamiltonian would be derived near a first order mean motion resonance and retaining only a single first order in eccentricity term using the Hamiltonian in equation 57. In this case the relevant frequency would be one of the following $\nu = \alpha_s^{-1}(2jn - 2(j+1)n' + \dot{\Omega})$, $\alpha_s^{-1}(2jn - 2(j+1)n' + \dot{\Omega}')$, $\alpha_s^{-1}(jn - (j+1)n' + \dot{\varpi})$ or $\alpha_s^{-1}(jn - (j+1)n' + \dot{\varpi}')$ depending upon the term. A Hamiltonian similar to 61 can also be derived near a third order mean motion resonance retaining only a single first order in eccentricity term and using the Hamiltonian in equation 56. In this case the relevant frequency would be $\nu = \alpha_s^{-1}(jn - (j+3)n' + \varpi)$ or $\alpha_s^{-1}(jn - (j+3)n' + \varpi')$.

Performing a canonical transformation with time dependent generating function that is a function of old coordinates and a new momentum

$$F_2(\phi, p', \tau) = \frac{1}{2}(\nu_2\tau + 2\phi)p', \quad (62)$$

giving new momentum $p' = p$ equal to the old one and a new angle

$$\varphi = \frac{1}{2}(\nu_2\tau + 2\phi). \quad (63)$$

Transforming the Hamiltonian in equation 61 we find a new Hamiltonian in these new coordinates

$$K(p,\varphi,\tau)_{c0j} = -\frac{p}{2}(2-p) + \frac{\nu_2 p}{2} + \epsilon p(2-p)\cos(2\varphi) \quad (64)$$

with

$$\epsilon \equiv \beta c_0^j. \quad (65)$$

The Hamiltonian is time independent as long as ν_2 is fixed, and ν_2 sets the distance to the center of resonance. We have neglected the phase c as it can be removed via shifting φ or τ.

We can write the frequency (equation 60)

$$\nu_2\frac{\alpha_s}{n} = j - (j+2)\left(\frac{a}{a'}\right)^{3/2}. \quad (66)$$

During an epoch of planet migration the semi-major axes a, a' may drift. When two planets approach each other either a increases or a' decreases so the frequency ν_2 decreases. If the planet orbits separate, ν_2 increases.

For various values of ν_2 level curves for the Hamiltonian in equation 64 are shown in Figure 1. There are no fixed points for $|\nu_2| > 2$. For $|\nu_2| < 2$ there are single stable fixed points at $\varpi = 0, \pi$ with p or θ value increasing with ν_2. The p value for the fixed points range from near 0 to near 2 corresponding to obliquity ranging from near 0 to near 180°.

We can mimic planet or satellite migration by allowing ν_2 to slowly vary. We let ν_2 be linearly dependent on time. We note that α_s, setting our unit of time and the strength of the coefficients, also depends on the semi-major axes. For the moment we regard them as constants and allow only ν_2 to vary. As ν_2 decreases, corresponding to the planets migrating so that they approach one another, a planet initially at low obliquity could be captured into a stable fixed point and lifted in obliquity. Using Hamilton's equations for Hamiltonian of equation 64 and $\epsilon = 0.01$, we integrated a planet or satellite, within initial low $p = 0.001$ (corresponding to an obliquity of $\theta = 2.6°$) and with $\dot{\nu}_2 = -0.001$. The time evolution of θ, φ are shown in Figure 3. The planet is captured into a resonant region near a fixed point and lifted to an obliquity of near 180° and then it escapes resonance. The resonance strength we used is small. Even when the resonance is weak and narrow, a planet or satellite could be captured into it and have its obliquity lifted to high values as the resonance frequency drifts.

3.2 Hamiltonian model for a perturbation proportional to $\sin\theta\cos\theta$

We now consider a Hamiltonian model with perturbation proportional to $\sin\theta\cos\theta$. We retain a single j term first order in inclination in the Hamiltonian 44. Using a frequency

$$\nu_2 \equiv \alpha_s^{-1}(jn - (j+2)n' + \Omega) \quad (67)$$

and a canonical coordinate transformation with generating function

$$F_2(\phi, p', \tau) = \frac{1}{2}(\nu_2\tau + \phi)p', \quad (68)$$

we derive a new angle

$$\varphi = \nu_2\tau + \phi \quad (69)$$

and a new Hamiltonian

$$K(p,\varphi,\tau)_{csj} = -\frac{p}{2}(2-p) + \nu_2 p + \epsilon(1-p)\sqrt{p(2-p)}\sin(\nu_2\tau + \phi) \quad (70)$$

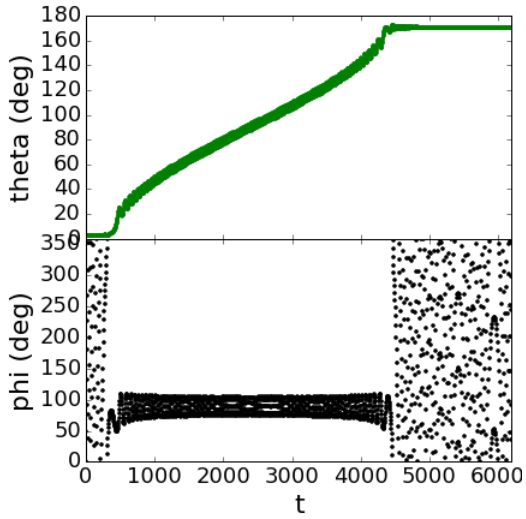

Figure 3. Integration of the Hamiltonian in equation 64 with a zero-th order perturbation (in inclination) $\propto \sin^2\theta$ and resonance strength $\epsilon = 0.01$. Here the resonance drifts with $\dot{\nu}_2 = -0.001$ corresponding to the planets slowly migrating closer together. Initial conditions are $(\varphi, p) = (1.5, 0.001)$, and $\nu_2 = 2.4$. The top panel shows obliquity as a function of time whereas the bottom panel shows the precession angle. The integrated body is captured into resonance at low obliquity and exits near an obliquity of 180°.

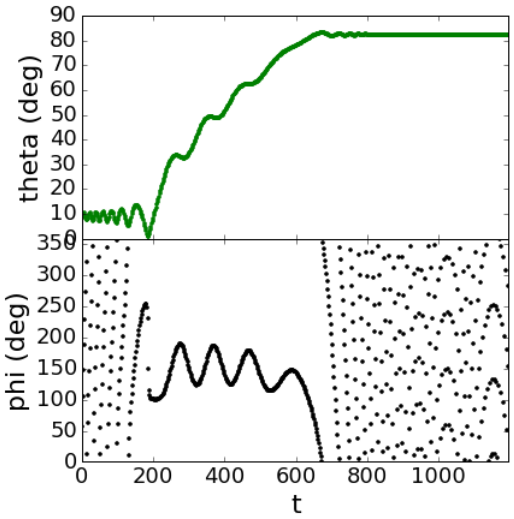

Figure 4. Integration of the Hamiltonian in equation 70 with a first order perturbation (in inclination) proportional to $\sin\theta\cos\theta$ and resonance strength $\epsilon = 0.01$. Here the resonance drifts with $\dot{\nu}_2 = -0.001$ for planets slowly migrating closer together. Initial conditions are $(\varphi, p) = (1.5, 0.001)$, and $\nu_2 = 1.4$. The top panel shows obliquity as a function of time whereas the bottom panel shows the precession angle. The integrated body is captured into resonance at low obliquity and exits near an obliquity of 90°.

with

$$\epsilon \equiv \beta c_s^j s. \tag{71}$$

The Hamiltonian would look the same if a first order term proportional to s' were used with frequency $\nu_2 = \alpha_s^{-1}(jn - (j+2)n' + \Omega')$ instead of $\alpha_s^{-1}(jn - (j+2)n' + \Omega)$, and the perturbation strength, ϵ, is proportional to $\beta c_{s'}^j s'$ instead of $\beta c_s^j s$. A similar Hamiltonian would be derived near a first order mean motion resonance and using a single j term that is first order in inclination from the Hamiltonian in equation 57.

Level curves for the Hamiltonian in equation 70 are shown in Figure 2 for different values of ν_2. For this Hamiltonian for $-1 < \nu_2 < 0$ a single fixed point is near $\varphi = 0$ and it has $p < 1$. However at $\nu_2 = 0$ the fixed point disappears and there are no fixed points. For $0 < \nu_2 < 1$ there is again a single fixed point but with $p > 1$.

As before we integrate the equations of motion for a slowly drifting system. We plot a planet trajectory in Figure 4 using the Hamiltonian in equation 70, $\epsilon = 0.01$, $\dot{\nu}_2 = -0.001$, initial conditions $(\varphi, p) = (1.5, 0.001)$ and $\nu_2 = 1.4$. Again we find that resonance capture is possible for a particle initially at low obliquity. However because the fixed point disappears near an obliquity of 90° the planet must escape resonance near this value rather than near 180° as for the perturbation that is proportional to $\sin^2\theta$ (explored in subsection 3.1).

3.3 Adiabatic Limits for Resonance Capture

When the drift from migration is too fast or not adiabatic, a particle in orbit will jump across mean motion resonance rather than capture into resonance (Quillen 2006). At drift rates below a critical drift rate, the resonance can capture at high probability. This critical drift rate is approximately equal to the square of the resonance libration frequency (Quillen 2006). There is a critical initial eccentricity, below which capture into mean motion resonance is assured when drift is adiabatic (Borderies & Goldreich 1984). The drift rate defining the adiabatic limit and the limiting eccentricity ensuring capture can be estimated from the Hamiltonian by considering the dimensions of the coefficients (Quillen 2006). By considering the form of the Hamiltonians in equations 64, 70 at low p we can similarly estimate the drift rate required for capture into spin resonance.

At low p (low obliquity) the perturbation term in the Hamiltonian of equation 64 (with perturbation $\propto \sin^2\theta$) is proportional to $\epsilon 2p\cos 2\phi$, so the drifting resonance behaves like a second order mean motion resonance that is proportional to e^2 or the Poincaré momentum variable Γ. The resonance libration frequency at low p is $\omega_{lib} \propto \epsilon$. In analogy to the Hamiltonian for mean motion resonance, we expect that capture into resonance for the drifting Hamiltonian of equation 64 is likely for drift rates $|\dot{\nu}_2| \lesssim \epsilon^2$ and for initial momentum $p \lesssim \epsilon$.

In contrast the resonant term for the Hamiltonian in 70, with perturbation $\propto \sin\theta\cos\theta$, at low p is proportional to $\sqrt{p}$ and so this resembles a first order mean motion resonance, proportional to e or the square root of the Poincaré momentum variable, $\sqrt{\Gamma}$. The libration frequency $\omega_{lib} \propto \epsilon^{\frac{2}{3}}$. The resonance should capture at a drift rate $|\dot{\nu}_2| \lesssim \epsilon^{\frac{4}{3}}$ and for initial $p \lesssim \epsilon^{\frac{2}{3}}$.

To estimate coefficients for the limits we show capture probabilities for a range of drift rates for the Hamiltonians in equations 64 and 70 in Figure 5. In both cases we set perturbation strength $\epsilon = 0.01$. We computed the capture probabilities for three different initial p values, 0.001, 0.01, and 0.1 corresponding to initial obliquities of 2.6, 8.1 and

26°. Each point shown in Figure 5 was computed from an average of 30 integrations where each integration was begun outside of resonance at a randomly chosen initial ϕ. To reduce dependence on phase we also chose random initial ν_2 values (but ensuring that we began outside of resonance). For those integrations that captured into resonance (as determined by a large increase in obliquity or p) we computed the mean final obliquity (of the integrations that captured) and these are shown as points on the bottom panels in Figure 5. The solid lines show fits of a tangent function to the capture probability.

Figure 5 shows that for low initial p capture takes place at $|\dot{\nu}_2| \sim 10^{-3}$ for the $\sin^2\theta$ resonance with Hamiltonian in equation 64. Using the dependence on ϵ^2 we estimate that

$$|\dot{\nu}_2|_{\sin^2\theta} \lesssim 10\epsilon^2 \tag{72}$$

for capture into the $\sin^2\theta$ resonance.

Capture takes place at $|\dot{\nu}_2| \sim 4\times10^{-3}$ for the $\sin\theta\cos\theta$ resonance (Hamiltonian of equation 70) giving

$$|\dot{\nu}_2|_{\sin\theta\cos\theta} \lesssim 2\epsilon^{\frac{4}{3}} \tag{73}$$

for capture into the $\sin\theta\cos\theta$ resonance.

The $\sin\theta\cos\theta$ resonance (Figure 5b) exhibits a sharper sensitivity to drift rate than the $\sin^2\theta$ one (Figure 5a), consistent with previous studies showing that first order mean motion resonances have a more abrupt transition in capture probability near the adiabatic limit (Quillen 2006).

Following resonance capture, Figure 5 shows that after escaping resonance the final obliquity is somewhat sensitive to initial obliquity and drift rate. For the $\sin^2\theta$ resonance, higher initial obliquity gave lower final obliquity after resonance capture. For both types of resonances, nearer the adiabatic limit and at higher drift rates, the final obliquities are lower.

How long does it take to lift the obliquity in one of these spin resonances? For the $\sin^2\theta$ resonance, once captured into resonance, p must drift from 0 to 2 but the coefficient $\propto p$ in the Hamiltonian in equation 64 contains a factor of 1/2. So the total time in resonance depends on $1/|\dot{\nu}_2|$. For the $\sin\theta\cos\theta$ resonance the total time in resonance is equivalent. Restoring units, once captured at low obliquity, the time to lift the obliquity to near 90° or near 180° for the $\sin^2\theta$ or $\sin\theta\cos\theta$ resonances, respectively is

$$T_{lift} \approx \frac{1}{|\dot{\nu}_2|\alpha_s}. \tag{74}$$

4 APPLICATION TO PLUTO AND CHARON'S MINOR SATELLITES

We consider spinning minor satellites Styx and Nix, that have orbits exterior to Charon. With an exterior spinning body, the unitless coefficient β (defined in equation 26) is approximately equal to the mass ratio of Charon and Pluto, $\beta \sim 0.1$. Styx is near the 3:1 resonance with Charon and Nix near the 4:1 resonance.

We first consider Styx, with an orbital period of 20 days. As Styx is near the 3:1 second order mean motion resonance we consider the Hamiltonian in equation 44 with $j = 1$. Inspection of Table 2 shows that there is a zero-th order (in inclination and eccentricity) perturbation with coefficient

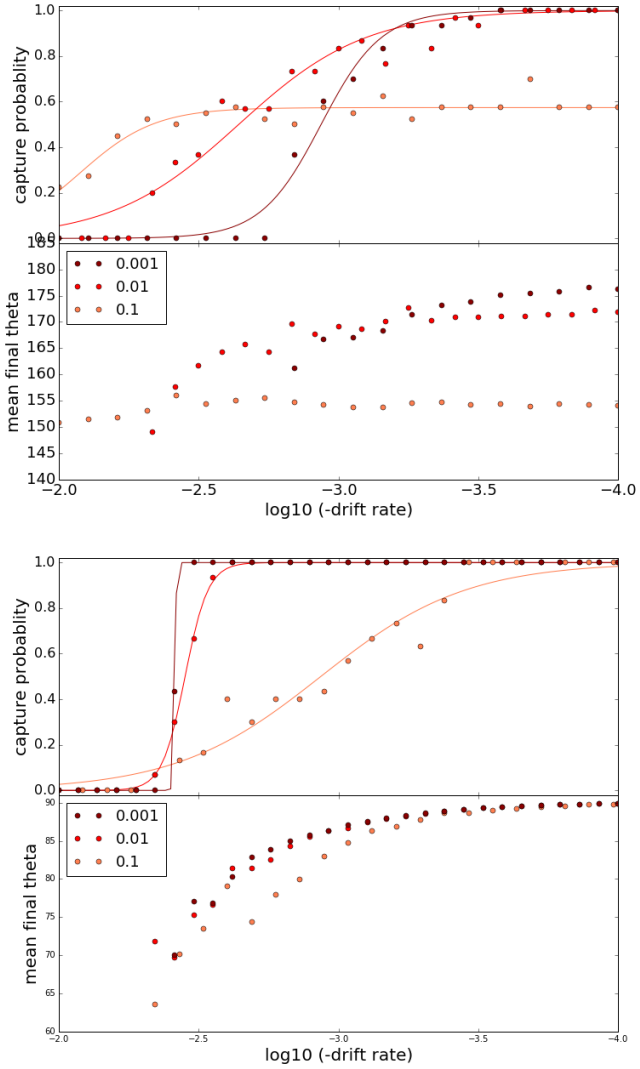

Figure 5. a) The top panel shows capture probabilities for the Hamiltonian in equation 64 with resonant term $\propto \sin^2\theta$ with resonance strength $\epsilon = 0.01$ as a function of drift rate for three different initial obliquities or p values. The initial p values 0.001, 0.01, 0.1, shown in the key on the lower left, correspond to initial obliquities of 2.6, 8.1 and 26°. The bottom panel shows the average final obliquities (in degrees) when capture took place for the same initial p values. The x axes show the $\log_{10}$ of the absolute value of the drift rate $|\dot{\nu}_2|$. The drift rate is higher on the left hand side and gives lower capture probabilities. Each point is computed from an average of 30 integrations. b) Similar to a) except for the Hamiltonian in equation 70 and with resonant term $\propto \sin\theta\cos\theta$.

$c_0^1(\alpha) = 0.76$ giving a resonance term $\propto \sin^2\theta$. There are two terms first order in orbital inclination that larger, $c_s^1 = 1.782$ and $c_{s'}^1 = -4.84$ and giving a resonance term $\propto \sin\theta\cos\theta$. The c_0 term need only be multiplied by β giving resonance strength $\epsilon = 0.1 \times 0.76 = 0.08$ for the Hamiltonian in equation 64. The c_s^1 and $c_{s'}^1$ coefficients should be multiplied by the orbital inclinations of Styx and Charon, respectively to estimate the strength of the $\sin\theta\cos\theta$ resonance. Working in a coordinate frame aligned with Styx's orbit (and with the

obliquity measured with respect to Styx's orbit normal), we use the inclination of Charon and need only the $c^1_{s'}$ coefficient. Taking into account $\beta = 0.1$, we estimate a resonance coefficient strength $\epsilon = 0.1 \times c^1_{s'} = 0.48 I_{Charon}$ where I_{Charon} is the inclination of Charon's orbit relative to Styx's. With an inclination of $I_{Charon} = 6^\circ = 0.1$ radians we find $\epsilon = 0.05$. The resonant perturbation term is $\propto \sin\theta\cos\theta$ and the relevant Hamiltonian is equation 70.

The two resonance strengths, $\propto \sin^2\theta$ and that $\propto \sin\theta\cos\theta$, have similar strengths when Charon's inclination is $\sim 8^\circ$. With a moderate inclination, the $c^1_{s'}$ resonance might be more important than the c^1_0 one. After capture, Styx should exit the $\sin\theta\cos\theta$ resonance with an obliquity near 90°, as we saw in our simulations (section 5 by Quillen et al. 2017) and as illustrated in Figure 4. In contrast after capture into the c_0 resonance, $\propto \sin^2\theta$, Styx should exit the resonance near an obliquity of 180°.

Which spin resonance is encountered by Styx first as Charon drifts away from Pluto? The two resonances are not on top of each other as the $\sin^2\theta$ resonance has argument with frequency $\nu_2\alpha_s = n_{Styx} - 3n_{Charon}$, whereas for the $\sin\theta\cos\theta$ resonance the argument frequency is $\nu_2\alpha_s = n_{Styx} - 3n_{Charon} - \Omega_{Charon}$. As $\dot{\Omega}_{Charon} < 0$, for an outward drifting Charon, Styx should encounter the $\sin\theta\cos\theta$ resonance first and that may explain why the obliquity was lifted to near 90° in our simulations rather than 180° (see section 5 by Quillen et al. 2017). At high obliquity, the $\sin^2\theta$ resonance could still be important. Perhaps this resonance, or evolution involving both perturbation terms could account for the higher than 90° obliquities of Nix and Hydra measured by Weaver et al. (2016).

With resonance strength $\epsilon \sim 0.05$ the drift rate in the $\sin\theta\cos\theta$ resonance (using equation 73) $|\dot{\nu}_2| \lesssim 0.04$ and giving a constraint on the migration rate $|\dot{n}| \lesssim 0.04\alpha_s^2$ or migration on a timescale $t_{mig} \gtrsim 30 \left(\frac{n}{\alpha_s}\right)^2 n^{-1}$. Here either Charon can move away from Pluto or equivalently Styx could migrate inward. As discussed in section 2.4 of Quillen et al. (2017), the precession rate for all the minor satellites is $\alpha_s \sim \frac{n}{2}\frac{P_s}{P_o}$ where $\frac{P_s}{P_o}$ is the ratio of spin period to orbital period. Currently $\frac{P_o}{P_s} \sim 6.2, 13.6$ for Styx and Nix, respectively. This gives a constraint on the migration timescale

$$t_{mig} = \frac{a}{\dot{a}} \gtrsim 30 \left(\frac{P_s}{P_o}\right)^2 P_o \tag{75}$$

or a few thousand times greater than the orbital period. This limiting migration rate is not slow and would be satisfied during an epoch of circumbinary disk evolution (e.g., Kenyon & Bromley 2014) . The total time required for the lift in obliquity to take place (using equation 74) would be only of order a hundred orbital periods or a few thousand years, easily satisfied, and consistent with the rapid obliquity lifts seen in our simulation.

Nix is near the third order 4:1 mean motion resonance and the Hamiltonian we consider is that in equation 56. The terms that are important are the coefficients that are first order in eccentricity, c^1_{e3} and $c^1_{e'3}$ and with $j = 1$. However this resonance is $\propto \sin^2\theta$ and our simulation showed resonance escape near an obliquity of $\sim 90^\circ$. We would attribute this behavior to higher order terms, proportional to es' that we neglected from our computations in section 2.5. However a comparison of terms in Table 2 suggests that the coefficients would be a few times larger than the c^1_{e3} or $c^1_{e'3}$ coefficients. We have checked that the expansion to first order in es' (or $e's'$) would give terms proportional to $\sin\theta\cos\theta$ and with argument similar to a third-order mean motion resonance. For the 4:1 resonance, dependence on inclination and eccentricity for the $\sin\theta\cos\theta$ term implies that the spin resonance strength would be weaker for Nix than Styx and so a slower migration rate and longer time would be needed to tilt Nix than Styx. However, the constraints on these quantities for Styx were not difficult to satisfy, so the mechanism for tilting Nix is also likely to be effective. If these spin resonances operated on Styx and Nix, the near 90° obliquities imply that Charon's orbit was relatively inclined during the migration as the strongest perturbation terms $\propto \sin\theta\cos\theta$ are first order in orbital inclination.

Our toy model considers each resonant term separately, but likely both $\sin^2\theta$ and $\sin\theta\cos\theta$ terms are present and simultaneously important for these spin resonances. We have not yet explored higher inclinations or slower migration rates in our mass-spring model simulations, leaving this for future work. At moderate inclination both Styx and Nix might initially be captured into a $\sin\theta\cos\theta$ resonance but escape or could be subsequently pushed higher by a $\sin^2\theta$ resonance, possibly accounting for Nix's 123° (Weaver et al. 2016) and higher than 90° obliquity.

Kerberos is near a 5:1 mean motion resonance with Charon and Hydra near a 6:1 mean motion resonance. Similar spin resonances could have operated on both of these satellites. Our Hamiltonian models in sections 2.4 and 2.5 imply that the spin resonances near the 5:1 and 6:1 mean motion resonances would be greater than first order in inclination and eccentricity. They would be weaker, require slower migration rates for capture and longer time to evolve within resonance to lift the obliquities.

We previously speculated that a mean motion resonance between Nix and Hydra could affect Hydra's obliquity (Quillen et al. 2017). However the strength of such a resonance depends on the mass ratio of Nix and Pluto and this would make the spin resonances 4 to 5 orders of magnitude weaker than those involving Charon. The resonance strengths computed here arise from the direct torque applied from a orbiting point mass, in this setting from Nix directly onto Hydra. Indirectly Nix could excite the orbit of Hydra due to a 3:2 first order mean motion resonance between them and the torque from Pluto and Charon arising from the orbit perturbations of Hydra might affect Hydra's spin. We have not yet computed this type of perturbation but suspect it would be most effective near a first order mean motion resonance (first order in eccentricity and between Nix and Hydra), as discussed at the end of section 2.5.

5 APPLICATION TO URANUS

The successful *Nice* model (Tsiganis et al. 2005) and its variants (e.g., Morbidelli et al. 2009; Nesvorny 2011; Nesvorny & Morbidelli 2012; Nesvorny 2015; Deienno et al. 2017), postulate an epoch or epochs of planetary migration beginning with planets near or in mean motion resonance (Morbidelli et al. 2007). During planet migration, secular resonances and

encounters between planets can alter planet spin orientation or obliquity (Ward & Hamilton 2004). Likewise the current obliquities of the giant planets could give clues about the extent and speed of planetary migration during early epochs of Solar system evolution (e.g., Boué & Laskar 2010; Brasser & Lee 2015).

The large obliquity of Uranus has primarily been attributed to a tangential or grazing collision with an Earth-sized proto-planet at the end of the epoch of accretion (e.g., Safronov 1969; Korycansky et al. 1990; Slattery et al. 1992; Lee et al. 2007; Parisi et al. 2008; Parisi 2011). However, Boué & Laskar (2010) proposed a collisionless scenario involving an additional, but now absent, satellite. Proposed is that a close encounter at the end of the era of migration ejected this satellite while Uranus was at high orbital inclination, leaving the planet at high obliquity following orbital inclination damping.

We consider the possibility that during an early epoch of planetary migration Uranus was captured into a mean motion resonance with another giant planet and while in it, its obliquity was lifted due to spin resonance. The spin resonance strengths (see equation 26) depend on the mass ratio of perturbing planet to that of the central star and this is at most the ratio of Jupiter's mass to that of the Sun or 10^{-3} . With Uranus external to Jupiter our parameter β is also decreased by the cube of the ratio of semi-major axes. The spin resonance strengths are likely to be 100 times weaker than we considered in the Pluto-Charon system, even taking into account the larger coefficients for first order mean motion resonances listed in Table 2. Furthermore equation 74 implies that the time required to lift Uranus would be of order 1000 times its precession period.

Taking into account its satellite system, Uranus's precession period is currently approximately 10^8 years (Ward 1975). The precession period is so slow that there is not enough time during a *Nice* model epoch of planetary migration for the spin resonances considered here to tilt the planet. If Uranus had a much heavier and more extended satellite system (Mosqueira & Estrada 2003a,b) then its precession period would be reduced. In this case we could consider capture into a 3:2 or 4:3 resonance with Saturn and a spin resonance associated with one of these mean motion resonances. However the resonance strengths depend on eccentricity and inclination, making them even weaker. The time required to lift the planet remains long, of order the age of the Solar system, requiring a timescale longer than the postulated era of migration. Uranus and Saturn migrating in such proximity are unlikely to remain stable and the spin resonance would require hundreds of spin precession periods to tilt Uranus. We conclude that the type of spin resonance explored here cannot account for Uranus's high obliquity.

The spin secular resonance mechanism explored by Ward & Hamilton (2004) involves drift of secular resonance. Uranus currently is near a secular resonance, the vertical secular eigenfrequency associated with Neptune, so the spin-secular resonance could have operated on a timescale of billions of years. For a mean-motion/spin precession to operate the planet would need to be near a mean motion resonance for billions of years but Uranus is no longer near one.

6 SUMMARY AND DISCUSSION

We have explored a Hamiltonian model for the dynamics of the principal axis of rotation of an orbiting planet or satellite assuming that the spinning body remains rapidly spinning about its principal inertial axis. We have computed the torque exerted on the spinning body from a point mass also in orbit about the central mass (a star if the our spinning object is a planet or a planet if our spinning object is a satellite). Unlike many previous studies (e.g., Colombo 1966), we do not average over the orbital period. We have computed perturbations from the point mass to first order in orbital inclination and eccentricity (but not their product). The perturbation terms are either proportional to $\sin^2\theta$ or to $\sin\theta\cos\theta$. Taking a single Fourier component (of the perturbation) we derive the Hamiltonians for the spin orientation shown in equations 44, 56, and 57 that are relevant near second order, third order and first order mean motion resonances, respectively, but affect obliquity and spin precession rate. The resonant arguments for the resonance near a second order mean motion resonance in equation 44 are consistent with slowly moving angles (equation 1) we previously saw in numerical simulations of Styx when its obliquity varied (Quillen et al. 2017). Our Hamiltonian model provides a framework for estimating the strengths of spin resonances involving a mean motion resonance and the precession angle of a spinning body.

Numerical integrations of one of these one-dimensional Hamiltonians (equations 44, 56, or 57) containing a single resonant perturbation term show that if the resonance drifts, a spinning body initially at low obliquity can be captured into spin resonance and its obliquity lifted to near 180° or 90° depending upon whether the perturbation term is $\propto \sin^2\theta$ or $\sin\theta\cos\theta$. The $\sin\theta\cos\theta$ requires non-zero orbital inclination of the spinning body with respected to the perturbing one. We estimate the maximum drift rate allowing spin resonance capture and the timescale required to reach the maximum obliquity when the body escapes resonance. Resonance capture into these spin resonances only takes place if the perturbing mass and spinning body have approaching orbits (similar to capture into mean motion orbital resonance).

We applied our Hamiltonian model to a migrating Pluto-Charon satellite system. The spin resonance seems capable of accounting for the large obliquity variations we previously saw in our simulations of the spin evolution of satellites Styx and Nix near the 3:1 and 4:1 mean motion resonances with Charon. Outward migration of Charon or inward migration of Styx and Nix would have allowed initially low obliquity Styx and Nix to be captured in to spin resonance and lift their obliquities. As Styx and Nix have obliquities near 90° and not near 180°, the capture would have involved a resonance proportional to $\sin\theta\cos\theta$ and so requires Charon's orbit to be inclined by a few degrees with respect to the orbits of Styx and Nix. Due to Charon's large mass, the resonances are sufficiently strong that the constraints on the migration rate for resonance capture are loose and the time needed to tilt the satellites is short, of order only a thousand years. Similar spin resonances could operate on Kerberos and Hydra, though they would be higher order in eccentricity and inclination and so weaker.

We explored whether Uranus could be tilted by a similar

mechanism during an early epoch when Uranus might have been in a first order mean motion resonance with another giant planet such as Saturn. However Uranus's spin precession period is long enough that tilting the planet would require billions of years. Since Uranus probably did not spend much time in or near mean motion resonance with another planet, this type of spin resonance is unlikely to account for Uranus's current high obliquity.

The type of spin-resonance explored here is weak for planets in the Solar system and so it was justifiably neglected from previous studies. However the spin-resonances discussed here may be important in migrating rapidly spinning satellite and planetary systems, such as Pluto and Charon's and possibly migrating compact exoplanet or satellite systems prior to tidal spin down. The approximate Hamiltonian model presented here could aid in interpretation of future simulations of spin evolution in such settings.

We explored toy Hamiltonian models containing a single resonant argument. However real systems are likely to be affected by multiple terms, each dependent on an argument that varies at a similar frequency. Spin evolution could be chaotic due to these nearby resonances. Interaction between the terms might allow resonance escape at obliquities between 90 and 180° possibly accounting for the 123° obliquity of Nix (Weaver et al. 2016). The spin resonances are important near mean motion resonances, and so future study of spin evolution where these spin resonances are important should also consider the orbital dynamics in or near mean motion resonance (e.g., Voyatzis et al. 2014).

We acknowledge helpful discussions with Santiago Loane and Benoît Noyelles if they are not collaborators. We gratefully acknowledge support from the Simons Foundation.

REFERENCES

Bills, B. G. 1990, The Rigid Body Obliquity History of Mars, J. Geophys. Res., 96, B9, 14137–14153.

Boué, G., & Laskar, J. 2006, Precession of a planet with a satellite, 2006, Icarus, 185, 312–330.

Borderies, N., & Goldreich, P. 1984, A simple derivation of capture probabilities for the j+1:j and j+2:j orbit-orbit resonance problems, Celest. Mech., 32, 127-132.

Boué, G., & Laskar, J. 2010, A Collisionless Scenario for Uranus Tilting, Astrophysical J. Letters, 712, L44-L47.

Brasser, R., and Lee, M. H. 2015, Tilting Saturn without Tilting Jupiter: Constraints on Giant Planet Migration, Astronomical J., 150, 157–175.

Colombo G. 1966, Cassini's second and third laws. Astronomical Journal, 71, 891–996.

Correia, A. C. M., Leleu, A., Rambaux, N., & Robutel, P. 2015, Spin-orbit coupling and chaotic rotation for circumbinary bodies; Application to the small satellites of the Pluto-Charon system, Astronomy and Astrophysics, 580, L14–21.

Deienno, R., Morbidelli, A., Gomes, R. S., Nesvorny, D. 2017, Constraining the Giant Planets? Initial Configuration from Their Evolution: Implications for the Timing of the Planetary Instability, Astronomical Journal, 153, 153–166.

Estrada, P. R., & Mosqueira, I. 2006, A gas-poor planetesimal capture model for the formation of giant planet satellite systems, Icarus, 181, 486–509.

French, R. G., et al. 1993, Geometry of the Saturn system from the 3 July 1989 occultation of 28 SGR and Voyager observations, Icarus, 103, 163–214.

Frouard, J., Quillen, A. C., Efroimsky, M., & Giannella, D. 2016, Numerical Simulation of Tidal Evolution of a Viscoelastic Body Modelled with a Mass-Spring Network, Monthly Notices of the Royal Astronomical Society, 458, 2890–2901.

Goldreich, P. 1965, Inclination of satellite orbits about an oblate precessing planet, Astronomical J., 70, 5–9.

Goldreich, P. and Toomre, A. 1969, Some Remarks on Polar Wandering, J. Geophys. Res., 74, 2555.

Goldreich, P., & S. J. Peale, S. J. 1966, Spin-orbit coupling in the solar system, Astronomical Journal, 71, 425–438.

Hamilton, D. P., & Ward, W. R. 2004, Tilting Saturn. II. Numerical Model, Astronomical J., 128, 2510—2517.

Kenyon, S. J., & Bromley, B. C. 2014, The Formation of Pluto's Low-Mass Satellites, Astronomical Journal, 147, 8–25.

Korycansky, D. G., Bodenheimer, P., Cassen, P., & Pollak, J. B. 1990, One-dimensional calculations of a large impact on Uranus, Icarus, 84, 528–541.

Laskar, J., & Robutel, P. 1993, The chaotic obliquity of the planets, Nature, 361, 608-612.

Lee, M. H., Peale, S. J., Pfahl, E., & Ward, W. R. 2007, Evolution of the obliquities of the giant planets in encounters during migration, Icarus, 190, 103–109.

Morbidelli, A., Tsiganis, K., Crida, A., Levison, H. F., & Gomes, R. 2007, Dynamics of the Giant Planets of the Solar System in the Gaseous Protoplanetary Disk and Their Relationship to the Current Orbital Architecture, Astronomical J., 134, 1790–1798.

Morbidelli, A., Brasser, R., Tsiganis, K., Gomes, R., & Levison, H. F., 2009, Constructing the secular architecture of the solar system I. The giant planets, Astron. & Astroph., 507, 1041–1052.

Mosqueira, I., & Estrada, P. R. 2003a, Formation of the regular satellites of giant planets in an extended gaseous nebula I: subnebula model and accretion of satellites, Icarus, 163, 198–231.

Mosqueira, I., & Estrada, P. R. 2003b, Formation of the regular satellites of giant planets in an extended gaseous nebula II: satellite migration and survival, 2003, Icarus, 163, 232–255.

Murray, C.D. & Dermott, S.F. 1999. Solar System Dynamics, Cambridge University Press, Cambridge.

Nesvorny, D. 2015, Evidence for Slow Migration of Neptune from the Inclination Distribution of Kuiper Belt Objects, Astronomical J., 150, 73–91.

Nesvorny, D. 2011, Young Solar System's Fifth Giant Planet? Astrophys. J., 742, L22–27.

Nesvorny, D., and Morbidelli, A. 2012, Statistical Study of the Early Solar System's Instability with Four, Five, and Six Giant Planets, Astronomical J., 144, 117–136.

Noyelles, B., Frouard, J., Makarov, V.V., and Efroimsky, M. 2014, Spin-orbit evolution of Mercury revisited, Icarus, 241, 26–44.

Parisi, M. G., Carraro, G., Maris, M., & Brunini, A. 2008, Constraints to Uranus' great collision IV. The origin of Prospero. Astron. & Astroph., 482, 657—664.

Parisi, M. G., & del Valle, L. 2011, Last giant impact on the Neptunian system. Constraints on oligarchic masses in the trans-Saturnian region, A&A, 530, A46

Parisi, M. G. 2011, Last giant impact on Uranus. Constraints on oligarchic masses in the trans-Saturnian region, Astron. & Astroph., 534, A28

Peale, S. J. 1974, Possible Histories of the Obliquity of Mercury Astronomical J., 70, 722–744.
Quillen, A. C., Nichols-Fleming, F., Chen, Y.-Y. and Noyelles, B. 2017, Obliquity evolution of the minor satellites of Pluto and Charon, Icarus, 293, 94–113.
Quillen, A. C. 2006, Reducing the probability of capture into resonance, Monthly Notices of the Royal Astronomical Society, 365, 1367–1382.
Rogoszinski, Z., & Hamilton, D. P. 2016, Tilting Uranus without a Collision, American Astronomical Society, DPS meeting #48, id. 318.09
Safronov, V. S. 1969, Evolution of the Protoplanetary Cloud and Formation of the Earth and the Planets, NASA TTF-677.
Slattery, W. L., Benz, W., & Cameron, A. G. W. 1992, Giant impacts on a primitive Uranus, Icarus, 99, 167–174.
Tsiganis, K., Gomes, R. , Morbidelli, A. & Levison, H. F. 2005, Origin of the orbital architecture of the giant planets of the Solar System, Nature 435, 459–461.
Touma, J., & Wisdom, J., 1993, The chaotic obliquity of Mars, Science, 259, 1294–1297.
Voyatzis, G., Antoniadou, K. I., and Tsiganis, K. 2014, Vertical instability and inclination excitation during planetary migration, CeMDA,119, 221–235.
Ward, W. R., 1973, Large-scale variations in the obliquity of Mars, Science, 181, 260–262.
Ward, W.R., 1974, Climatic variations on Mars: I. Astronomical theory of insolation, J. Geophys. Res. 79, 3375–3386.
Ward, W.R., 1975, Tidal friction and generalized Cassini's laws in the solar system, Astronomical J., 80, 64–70.
Ward, W. R., & Hamilton, D. P. 2004, Tilting Saturn. II. Analytical Model, Astronomical J., 128, 2501—2509.
Ward, W. R. 1979, Present obliquity oscillations of Mars: Fourth-order accuracy in orbital e and I, J. Geophys. Res. 114, 237–241.
Ward, W. R., and Rudy, D. J. 1991, Resonant obliquity of Mars? Icarus, 94, 160–164.
Ward, W. R., & Canup, R. M. 2006, The Obliquity of Jupiter, Astrophys. J. Letters, 640, L91–L94.
Weaver, H. A. et al. 2016, The Small Satellites of Pluto as Observed by New Horizons, Science, 351, 1281, DOI: 10.1126/science.aae0030
Wisdom, J., Peale, S. J., & Mignard, F. 1984, The Chaotic Rotation of Hyperion, Icarus, 58, 137–152.